Smart GFM Inverter Design and HIL Validation for Stability Support in Small-Scale PV Systems

Varun Nand
Dept. of Electrical & Electronic Engineering
Auckland University of Technology
Auckland, New Zealand
hjq8455@autuni.ac.nz

Shuai Zhou
Dept. of Electrical & Electronic Engineering
Auckland University of Technology
Auckland, New Zealand
zoey.zhou@aut.ac.nz

Tek Tjing Lie
Dept. of Electrical & Electronic Engineering
Auckland University of Technology
Auckland, New Zealand
tek.lie@aut.ac.nz

***Abstract*—The increasing penetration of inverter-based resources (IBRs) has intensified the need for smart inverters capable of supporting power system stability in microgrids with high levels of distributed PV generation. This paper presents the design and hardware-in-the-loop (HIL) validation of a droop-controlled grid-forming (GFM) inverter for a 100kW photovoltaic (PV) system. A high-fidelity model of the PV array, converter interface, and grid coupling was implemented in MATLAB/Simulink and executed in real time on an OPAL-RT OP5700 platform. This inverter was evaluated under islanded and grid-connected conditions through step-load disturbances, three-phase short-circuit faults, and low-voltage ride-through (LVRT) compliance testing. Results show that the inverter maintains stable frequency and voltage during small disturbances, recovers within 0.5s after a three-phase short-circuit fault without load shedding, and satisfies the New Zealand Grid Code LVRT requirement without the use of FACTS devices. These findings demonstrate the feasibility of small-scale GFM inverters to contribute ancillary services and improve stability in renewable-dominated microgrids.**

Keywords—Grid Forming (GFM) Inverter, Droop Control, Hardware-in-the-loop (HIL), PV systems, stability analysis

I. INTRODUCTION

The growing global demand for energy and the need to meet international carbon-emission targets have accelerated the deployment of inverter-based resources (IBRs), such as solar photovoltaic (PV) and wind generation systems [1]. This transition has fundamentally altered the topology of modern power systems, shifting from predominantly centralized generation toward highly distributed architecture composed of numerous small-scale units, including rooftop solar and commercial PV installations. While this paradigm shift supports decarbonization, it also introduces significant challenges to system stability and grid connection.

Most small-scale distributed energy resources (DERs) employ grid-following (GFL) control due to their limited capacity. Consequently, they are unable to provide essential ancillary services, such as frequency and voltage regulation, and lack fault tolerance mechanisms including low-voltage ride-through (LVRT) capability [2]. Historically, these functions were supplied by large synchronous generators; however, as fossil-fuel plants are retired and renewable penetration increases, DERs now account for a substantial portion of total generation. This shift has driven the development of advanced interconnection standards, such as IEEE 1547-2018, which introduce stricter requirements for voltage support, frequency response, and fault-ride-through capability [3]. Countries such as Australia and New Zealand are actively incorporating these requirements into their regulatory frameworks.

To address stability concerns in IBR-dominated networks, grid-forming (GFM) inverters have emerged as a key technology for improving stability in IBR-dominated networks, as they can autonomously establish voltage and frequency references and provide synthetic inertia [4]. At utility scale, GFM inverters are often deployed alongside flexible AC transmission system (FACTS) devices, such as static synchronous compensators (STATCOMs), to achieve dynamic voltage regulation and enhance system stability during disturbances [5]. However, the high capital cost and MVar-scale operating range of FACTS devices make them impractical for microgrids and small-scale DERs, while research into low-capacity STATCOM alternatives remains ongoing [6].

A summary analysis of market trends and investments in renewable energy suggests that IBRs are broadly categorized in one of two sets [7]. Expensive large-scale plants that use grid forming inverters in conjunction with FACTS devices to achieve regulation, stability and fault tolerance. The cheaper small-scale plants that use grid following inverters to provide power but rely on the grid for regulation and stability and offer minimal fault tolerance characteristics. The proliferation of solar on the grid has in recent years led to stability issues that have resulted in massive power outages incurring both equipment and economic damage. In Australia the energy regulatory body has sought legal action against suppliers for failing to meet LVRT compliance during the 2016 South Australian System Blackout [8]. Subsequent analysis reports have indicated that the proliferation of low-cost rooftop solar without incorporating sufficient ancillary services poses a major risk to the grid akin to the 2016 South Australian blackout event [9]. The goal of this research is to bridge this gap by addressing core issues around regulation, stability and fault tolerance by designing and validating the design of a small utility scale smart inverter that has grid forming capabilities.

978-1-6654-1819-5 /22/$31.00

This research aims to address these limitations by developing and experimentally validating a GFM smart inverter capable of providing frequency and voltage regulation and achieving grid-compliant LVRT without reliance on any load shedding or FACTS devices. The inverter is designed to meet the ancillary-service and stability requirements of the New Zealand Grid Code, offering a practical pathway for enabling small-scale DERs to contribute to grid stability.

The key contributions of this research are as follows:

1. Development of a droop-controlled GFM PV inverter capable of autonomously regulating frequency and voltage in both islanded and grid-connected operation.
2. Hardware-in-the-loop (HIL) validation of steady-state stability under step-load disturbances, demonstrating stable operation within grid-code frequency and voltage limits.
3. Real-time demonstration of transient stability, with full recovery from a three-phase short-circuit- fault without load shedding and any FACTS devices.
4. Verification of LVRT performance for the New Zealand Grid Code, achieved without reliance on any FACTS devices.

The remainder of this paper is organized as follows. Section II presents the system model of PV systems. Section III describes the proposed droop control-based GFM implementation. Section IV details the HIL simulation platform setup, and the real-time simulation results. Section V provides conclusion and potential future work.

II. System Model

A. System Architecture

The core system consists of a solar PV array, a DC-DC boost converter implementing maximum power point tracking (MPPT), and a three-phase inverter operating under droop-controlled GFM control. The PV array supplies DC power to the MPPT-based boost converter, which regulates the DC-link voltage and ensures extraction of maximum available solar power. The regulated DC power is then fed to the three-phase inverter, which establishes voltage and frequency references through droop control to enable autonomous operation in both islanded and grid-connected modes.

The inverter output is passed through an L-C filter to attenuate switching harmonics and generate low distortion three-phase AC waveforms suitable for grid interfacing. The filtered AC output is connected to the point of common coupling (PCC), which is the connecting point between the PV system and grid. This allows the PV system to interact with local loads or the utility grid. The overall system structure is illustrated in Fig. 1.

B. Core Specification

The system specifications were selected to reflect the characteristics of small-scale commercial and agricultural PV installations commonly found in New Zealand. Such installations typically employ GFL inverters that depend on the utility grid for voltage and frequency stability. In contrast, this study replaces the conventional GFL interface with a GFM inverter to evaluate its ability to provide autonomous regulation and enhanced stability. Because commercially available GFM inverters are generally designed for medium- to large-scale applications, a 100kW PV system, which is a representative of upper-range commercial rooftop installations, was chosen as a practical test case.

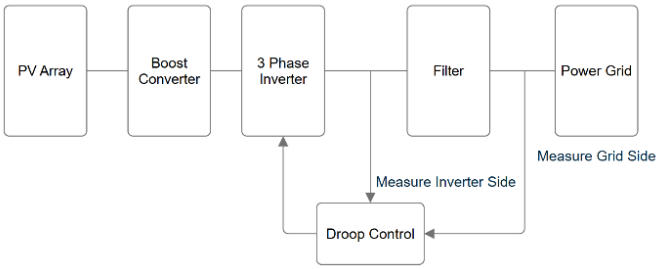

Fig 1: Overall System Structure

1. 100kW PV array, typical of commercial rooftop systems operating under power purchase agreements in New Zealand.
2. MPPT Based DC-DC boost converter, selected to maximize energy extraction and maintain DC-link stability [10].
3. LCL output filter, providing cost-effective design with superior harmonic attenuation that provides improved power quality [11]
4. Droop-controlled GFM inverter, designed to enhance voltage and frequency regulation while improving system fault tolerance.

III. Grid Forming Control Implementation

The proposed GFM controller adopts a hierarchical droop-based architecture consisting of coordinated voltage and current control loops. The controller regulates the inverter output in a synchronous reference frame (SRF) using real-time measurements of three-phase voltages and currents at the LCL filter output. These measurements are transformed into the dqframe, enabling decoupled control of active and reactive power.

The outer control loop emulates the behavior of a synchronous generator by applying frequency and voltage droop characteristics. Based on the measured active and reactive power, the controller computes the reference frequency and voltage magnitude required to maintain stable operation under varying load conditions. The inner current-control loop tracks these reference values using SRF-based PI regulators, ensuring fast dynamic response and accurate current shaping [12, 13]. Together, these loops allow the inverter to autonomously regulate voltage and frequency under both grid-connected and islanded operation.

A. Mathematical Modelling

The droop controller is formulated based on the instantaneous active and reactive power derived from the measured dq-axis voltages and currents at the inverter output.

The three-phase AC voltage and current signals are first converted into the stationary $\alpha\beta$ frame using the Clarke transformation. These $\alpha\beta$ components are then transformed into the rotating dq frame using the Park transformation. The block diagram illustrating the Clarke and Park transformations, along with the mathematical operations used to obtain the dq-components from the three-phase AC signals, is shown in Fig. 2. In this manner, the three-phase signals are reduced to two orthogonal components that are used for control.

The resulting dq voltages and currents, denoted v_d, v_q, i_d, i_q, are used to calculate active and reactive power:

$$P = \frac{3}{2}\left(v_d i_d + v_q i_q\right) \qquad (1)$$

$$Q = \frac{3}{2}\left(v_q i_d - v_d i_q\right) \qquad (2)$$

where, v_d and v_q are the d- and q-axis components of the inverter output voltage, and i_d and i_q are the corresponding d- and q-axis components of the output current obtained through the synchronous reference frame transformation.

The droop laws for frequency and voltage modulation are defined as:

$$f = f_n - m_p(P - P_o) \qquad (3)$$

$$V = V_n - m_q(Q - Q_o) \qquad (4)$$

where,

f and V are the frequency and voltage magnitude;

f_n and V_n are reference setpoints;

P_o and Q_o represent nominal operating power;

m_p and m_q are the active- and reactive-power droop coefficients.

B. Droop Control

The droop control algorithm adjusts the inverter's operating frequency and voltage based on deviations of measured active and reactive power from their respective reference values. A droop coefficient m_p is applied to the difference between the calculated and reference active power, and the resulting value is subtracted from the nominal reference frequency f_n to generate the new operating frequency of the inverter. Similarly, a droop coefficient m_q is applied to the difference between the calculated and reference reactive power, and the resulting value is subtracted from the nominal reference voltage V_n to generate the new operating voltage [14, 15].

The operating voltage directly sets the amplitude of the inverter's output AC signal, while the operating frequency determines the output AC signal frequency. The resulting frequency and voltage references are then transformed into the dq frame and fed to the voltage and current control loops of the inverter. These loops track the droop-modified references and produce the final dq output signals. The block diagram of the overall grid-forming inverter design, including the droop control and inner voltage/current loops, is shown in Fig. 3. Finally, an inverse dq transformation converts these signals into three-phase quantities that generate the PWM duty cycles for controlling the IGBT switches of the inverter [16].

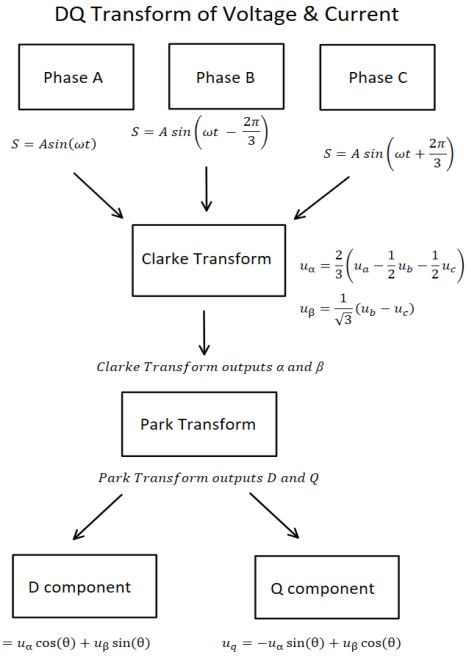

Fig 2: Block Diagram of dq Transformation Mathematical Operations

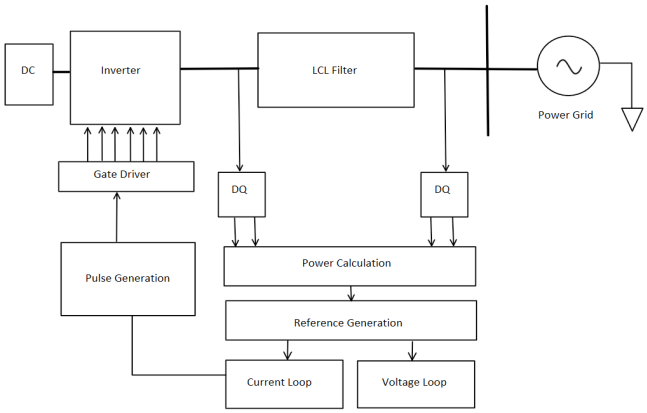

Fig 3: Block Diagram of the Grid Forming Inverter Design

The specification of the core parameters of the system design can be seen in table 1 below. It lists the values used for LCL filtering, the droop coefficients applied to the system and controller coefficients for the voltage and current controller.

TABLE I. CORE DESIGN PARAMETERS

Key Parameter	**Table Column Head**		
	Description	***Value***	***Units***
L1	LCL inverter side inductor	1.2	*mH*
L2	LCL grid side inductor	600	*mH*

Key Parameter	Table Column Head		
	Description	*Value*	*Units*
C1	LCL capacitor	80	*uF*
m_p	Frequency Droop Coefficient	31.41e-5	-
m_q	Voltage Droop Coefficient	50e-6	-
P_v	Voltage Loop P-Gain	0.1	-
I_v	Voltage Loop I-Gain	100	-
P_c	Current Loop P-Gain	30.1	-
I_c	Current Loop I-Gain	300	-

IV. HIL VALIDATION RESULTS

The system developed in this research was designed to capture the practical constraints associated with implementing a full-scale smart inverter for a small-scale PV system. To validate the proposed grid-forming droop control, an end-to-end model of a 100kW PV installation, from the PV array through the inverter interface to the grid connection, was implemented in MATLAB/Simulink. All major subsystems, including the PV generation subsystem, DC-DC interface, inverter control loops, and grid-coupling elements, were modelled with power electronics-level fidelity to accurately represent system dynamics.

HIL test was performed using an OPAL-RT OP5700 real-time simulator with the RT-Lab software environment. This real-time execution setup allows closed-loop interaction between the inverter controller and the simulated PV system, enabling high-fidelity evaluation of both steady-state and transient responses without the cost or risk associated with full-scale hardware deployment. Fig. 4 illustrates the HIL setup, including the OP5700 simulator, a digital storage oscilloscope (DSO), and the host machine running RT-Lab software.

To evaluate the inverter's contribution to system stability and grid support, the following tests were conducted under both islanded and grid-connected operation:

(1) Steady-state stability analysis: a step change in load was applied to observe the droop-controlled inverter's ability to regulate frequency and voltage.

(2) Transient stability analysis: a three-phase short-circuit fault was introduced at PCC.

(3) LVRT performance: the inverter's LVRT response was evaluated against New Zealand Grid Code requirements.

A. Steady-state Stability Analysis

In steady-state stability analysis, a step change in load was applied in both islanded and grid-connected configurations at t = 4s. The results have been compared to the frequency and voltage requirements in New Zealand Grid Code.

1. Islanded Mode

Fig. 5 illustrates the inverter response when a load is switched on at t = 4s during isladed operation. The system exhibits a small frequency drop and a light RMS voltage dip, both characteristic of droop-controlled frequency-voltage regulation. These deviations remain well within the droop-control limits specified for autonomous operation. Following the disturbance, the inverter rapidly restores frequency to within the allowable 49.25 - 50.75 Hz and maintain RMS line voltage within ±5% of 1.0 pu, which are specified in New Zealand Grid Code. Furthermore, active and reactive power outputs rise proportionally to supply the increased load, and little oscilalations and overshooot are observed. These results confirm stable frequency-voltage regulation in standalone operation.

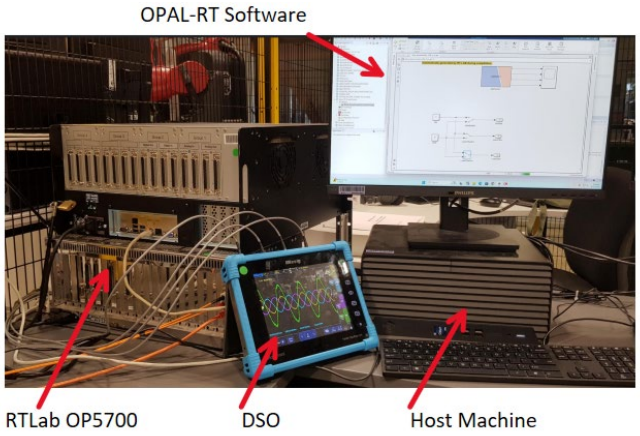

Fig 4: HIL Setup of Real-time Validation

2. Grid-connected Operation

Fig. 6 shows the corresponding response for the grid-connected configuration. When the load is applied at t = 4s, the inverter again produces the expected droop-based response, including a minor frequency dip and a small voltage deviation, both significantly damped due to the stiff grid forming the infinite bus. The inverter increases active power output smoothly and regulates reactive power to maintain voltage at PCC. Power and voltage settle quickly, demonstrateing reliable disturbance rejection while synchronized to the grid.

In both islanded and grid-connected steady-state conditions, frequency and voltage remain within their New Zealand Grid Code compliance envelopes.

B. Transient Stability Analysis

In transient stability analysis, a three-phase short-circuit fault was applied at PCC. The system was tested under both islanded and grid-connected modes. The fault was applied to the systems at t = 6s, and cleared after 0.14s which is used to meet the grid code LVRT requirement.

1. Islanded Mode

Fig. 7 presents the islanded-mode response, showing the frequency trajetory and RMS line voltage waveform during and after the fault. When the fault is initiated, the RMS voltage collapses as expected, and the inverter reduces active power output whiel providing reactive support. Despite the severe disturbance, the inverter maintains stable freuqncy control and does not disconnect.

Once the fault was cleared after 0.14s, the system exhibited full recovery within 0.5s, returning both frequency and RMS

voltage to their nominal values without any load shedding. This confirms that the smart inverter can sustain stable autonomous operation through severe faults.

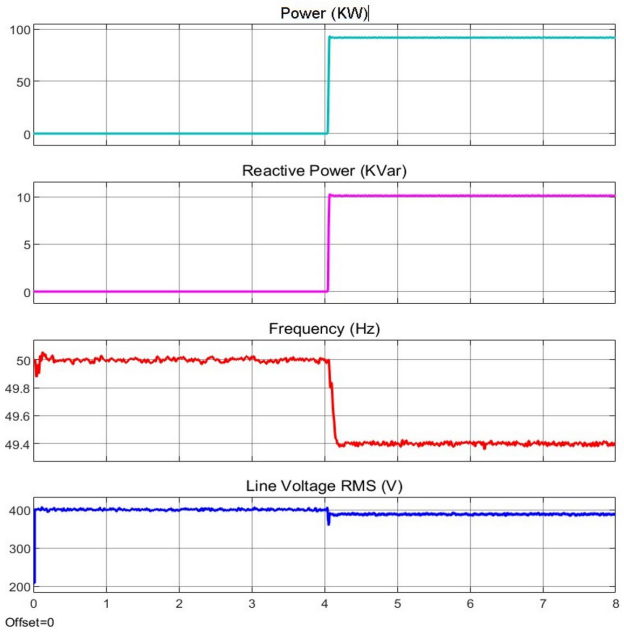

Fig 5: Steady-state Response in Islanded PV System

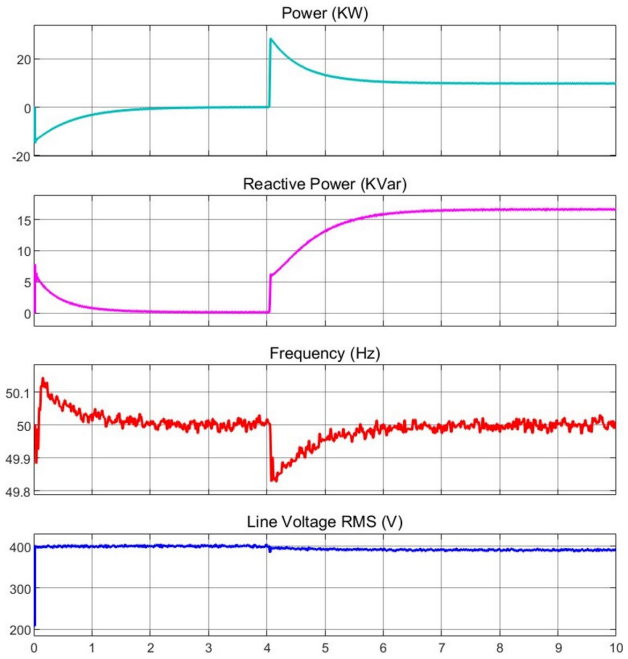

Fig 6: Steady-state Response in Grid-connected PV System

2. Grid-connected Operation

Fig. 8 shows the corresponding response in the grid-connected configuration. The stiff grid reference helps maintain synchronization, and the inverter continues to regulte voltage and reactive power during the fault. RMS voltage again collapses during the fault but recovers rapidly once the fault is cleared.

Similar to the islanded case, the system achieves complete recovery within 0.5s, with no loss of synchronism and no load shedding. Active power and voltage return smoothly to their pre-fault leves, demonstrating strong dynamic stability under grid-side faults.

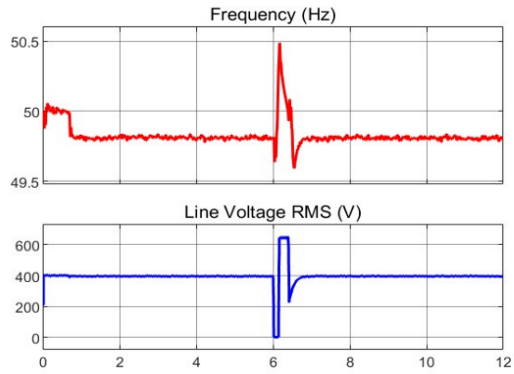

Fig 7: Transient Response in Islanded PV System

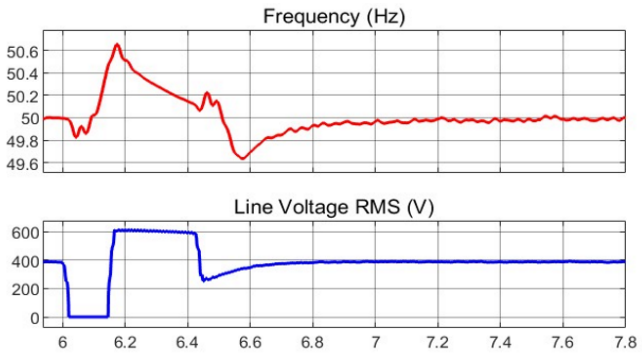

Fig 8: Transient Response in Grid-connected PV System

C. *LVRT Compliance*

The system's LVRT capability was evaluated against the New Zealand Grid Code requirements, which specifies the following minimum voltage recovery thresholds: (1). 0.35 pu within 0.5s; (2) 0.76 pu within 1.3s; (3) 0.90 pu within 3.0 s of the post-fault event [17].

Fig. 9 shows the voltage recovery trajectory of the grid-connected PV system with proposed smart inverter (blue line). The voltage at PCC reaches 0.98 pu within 0.5s, significantly faster than the minimum requirement. This demonstrates that the system fully satisfies New Zealand LVRT criteria (red line) without requiring any FACTS devices. The system remains connected throughout the event, highlighting the effectiveness of the proposed GFM control strategy during severe fault scenarios.

V. CONCLUSION

This paper presented the design and real-time validation of a droop-controlled GFM smart inverter for small-scale PV systems. The proposed inverter was tested using a HIL platform to evaluate its performance under both steady-state and transient operating conditions in islanded and grid-connected configurations.

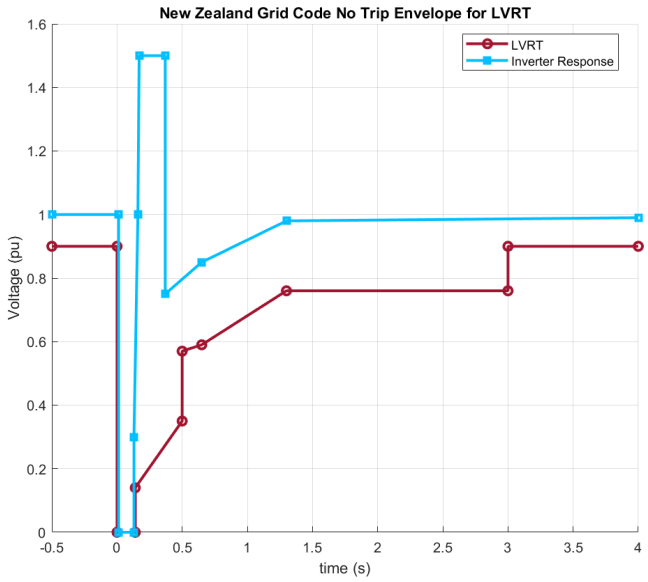

Fig 9: LVRT Capability within the NZ Grid Code No Trip Envelope

The key findings from the HIL simulations are as follows:

1. Steady-state stability: step changes in load demonstrated that the droop-controlled inverter can regulate frequency and voltage effectively in both islanded and grid-connected modes. Frequency deviations remained within 49.25 – 50.75 Hz, and RMS voltage stayed within ±5% of 1.0 pu, confirming reliable steady-state stability.

2. Transient stability: During three-phase short-circuit faults, the inverter-maintained synchronization supported voltage through reactive power injection and restored both frequency and voltage to nominal values within 0.5s without load shedding, demonstrating robust transient performance in both operating modes.

3. LVRT capability: the inverter successfully met the New Zealand Grid Code LVRT requirements, recovering voltage to 0.98 pu within 0.5s, significantly exceeding the minimum envelope specified by the standard.

The results collectively show that the proposed droop control-based GFM inverter can provide ancillary services, maintain system stability, and support grid reliability for small-scale PV installations. Future work will focus on extending these results to larger-scale microgrids, optimizing controller parameters for enhanced dynamic performance, and evaluating system-wide interactions using standard test networks. These studies will further support the deployment of smart inverters to improve system stability in renewable-dominated grids.

ACKNOWLEDGEMENT

This research is supported by the AUT-CNBM Intelligent Green Technology Research Hub.

REFERENCES

[1] International Energy Agency. (2025, June 6). *Global energy investment set to rise to $3.3 trillion in 2025 amid economic uncertainty and energy security concerns*. https://www.iea.org/news/global-energy-investment-set-to-rise-to-3-3-trillion-in-2025-amid-economic-uncertainty-and-energy-security-concerns

[2] Hasheminasab, S., Alzayed, M., & Chaoui, H. (2024). A review of control techniques for inverter-based distributed energy resources applications. *Energies*, *17*(12), 2940.

[3] Photovoltaics, D. G., & Storage, E. (2018). IEEE standard for interconnection and interoperability of distributed energy resources with associated electric power systems interfaces. *IEEE Std*, *1547*(1547), 2018.

[4] Gao, X., Zhou, D., Anvari-Moghaddam, A., & Blaabjerg, F. (2023). A comparative study of grid-following and grid-forming control schemes in power electronic-based power systems. *Power Electronics and Drives*, *8*, 1-20.

[5] Ibram, D., & Gueorgiev, V. (2021, September). Reactive power compensation in grid connected photovoltaic system using static synchronous compensator. In *2021 13th Electrical Engineering Faculty Conference (BulEF)* (pp. 1-5). IEEE.

[6] Yuan, Y., Zhou, J., Zhang, Y., Zhao, X., & Xu, G. (2022). Low-capacitance cascaded H-bridge STATCOM for full power operation. *Journal of Power Electronics*, *22*(2), 287-296.

[7] Fortune Business Insights. (2026, January). Grid-Forming Inverter Market Size & Forecast. https://www.fortunebusinessinsights.com/grid-forming-inverter-market-109817

[8] Austrian Energy Regulator. (2022, June 28). AER Media News Release, AGL Penalties for Breaching Energy Rules.

[9] Austrian Energy Regulator. (2016, September 28). System Blackout Compliance Report.

[10] Singh, S., Manna, S., Mansoori, M. I. H., & Akella, A. K. (2020, July). Implementation of perturb & observe MPPT technique using boost converter in PV system. In *2020 international conference on computational intelligence for smart power system and sustainable energy (CISPSSE)* (pp. 1-4). IEEE.

[11] Kim, Y. J., & Kim, H. (2019). Optimal design of LCL filter in grid-connected inverters. *IET Power Electronics*, *12*(7), 1774-1782.

[12] Miranda, U. D. A., Rolim, L. G. B., & Aredes, M. (2005, June). A DQ synchronous reference frame current control for single-phase converters. In *2005 IEEE 36th power electronics specialists conference* (pp. 1377-1381). IEEE.

[13] Petrella, R., Revelant, A., & Stocco, P. (2009, September). Robust grid synchronization in three-phase distributed power generation systems by synchronous reference frame pre-filtering. In *2009 44th International Universities Power Engineering Conference (UPEC)* (pp. 1-5). IEEE.

[14] Mhankale, S. E., & Thorat, A. R. (2018, March). Droop control strategies of DC microgrid: A review. In *2018 International Conference on Current Trends towards Converging Technologies (ICCTCT)* (pp. 372-376). IEEE.

[15] Zhang, W., Zheng, Z., & Liu, H. (2021). Droop control method to achieve maximum power output of photovoltaic for parallel inverter system. *CSEE Journal of Power and Energy Systems*, *8*(6), 1636-1645.

[16] Guo, W., & Mu, L. (2016). Control principles of micro-source inverters used in microgrid. *Protection and Control of Modern Power Systems*, *1*(1), 5.

[17] New Zealand Electricity Authority (Update June 2025). Electricity Industry Participation Code 2010. *Section 8 Common Quality*. *https://www.ea.govt.nz/code-and-compliance/the-code-electricity-industry-participation-code-2010/*

[18] Prabhakaran, P., Goyal, Y., & Agarwal, V. (2017). Novel nonlinear droop control techniques to overcome the load sharing and voltage regulation issues in DC microgrid. *IEEE Transactions on power electronics*, *33*(5), 4477-4487

[19] Chen, F., Burgos, R., Boroyevich, D., Vasquez, J. C., & Guerrero, J. M. (2019). Investigation of nonlinear droop control in DC power distribution systems: Load sharing, voltage regulation, efficiency, and stability. *IEEE Transactions on Power Electronics*, *34*(10), 9404-94